Free surface Hele-Shaw flows around an obstacle: A random walk simulation

Vladislav A. Bogoyavlenskiy* and Eric J. Cotts
Physics Department, State University of New York at Binghamton, Binghamton, New York 13902-6016, USA
(Received 30 September 2002; revised manuscript received 8 October 2003; published 29 January 2004)

This paper presents computer simulations of pressure driven viscous flows that creep in two dimensions (Hele-Shaw cells). We model the time and spatial evolution of free liquid-gas interfaces perturbed by solid obstacles of various configurations such as wedges, steps, and ellipses. Our goal is to study short- and long-scale obstacle effects on the interface shape and velocity. Specific focus is given to the dynamics of a triple (gas-liquid-solid) contact line, which determines local wetting of obstacles. As a principal contribution, we derive a functional relationship between the contact line velocity and the obstacle geometry.

DOI: 10.1103/PhysRevE.69.016310 PACS number(s): 47.15.Gf, 47.11.+j, 68.03.−g, 83.50.−v

I. INTRODUCTION

The complex time development of a free interface that separates immiscible fluids in a two-dimensional geometry (Hele-Shaw cell [1]) has been the subject of extensive theoretical and experimental studies since the end of the nineteenth century [2]. In this field, most of the research attention is addressed to *unstable* cases of the interface evolution, such as gravitational and viscous instabilities that were originally captured by Lord Rayleigh, Taylor, and Saffman [3–5]. Surprisingly, the opposite situation of *stable* Hele-Shaw hydrodynamics is much less investigated. The reason stems from a seeming triviality of stable cases—the moving interface is imagined to be simply flat and normal to a flow direction, with no peculiarities—which is not always realized.

In the present work, we consider the problem of a uniform pressure-induced replacement of an inviscid fluid (gas) by a viscous one (liquid) in a plane Hele-Shaw cell; the related free-boundary formalism definitely yields stable solutions [6]. The interface between liquid and gas is expected to creep flat until we superimpose a solid obstacle for the flow—it should cause a spatial disturbance and, as a consequence, global curvature of the moving interface. Our goal will be to investigate the dynamics of this flow-obstacle interaction on both short and long length scales. Besides its fundamental importance, such a problem has direct relevance to engineering applications, e.g., in manufacturing of electronic devices [7].

The rest of this paper is organized as follows. In Sec. II we introduce a mathematical formulation for liquid-gas interfaces creeping in Hele-Shaw cells around solid obstacles. After that in Sec. III we describe a numerical technique applied for modeling the free surface Hele-Shaw flows, a random walk simulation. Next in Sec. IV we report numerical data on the interface dynamics for various obstacle configurations such as (a) wedges, (b) steps, and (c) ellipses. In Sec. V we discuss the results obtained, deriving a general formula for the velocity of a triple (gas-liquid-solid) contact line, which determines local wetting of obstacles. Finally, conclusions are provided in Sec. VI.

II. MATHEMATICAL FORMULATION

Let us consider a liquid-gas interface creeping around a solid obstacle in a plane Hele-Shaw cell (see Fig. 1). Assuming a thickness b of the cell to be infinitesimal in comparison with its length and width, hydrodynamic equations for the velocity $\mathbf{v}(\mathbf{r},t)$ and the pressure $p(\mathbf{r},t)$ fields become effectively two dimensional, as for $\mathbf{r}=(x,y)$ [5]. We consider our Hele-Shaw flow to be driven by a pressure gradient (for instance, due to capillary action at free surface), dissipating by the shear viscosity μ. So, in liquid bulk one has to solve Laplace's incompressibility law

$$\nabla^2 p(\mathbf{r},t)=0 \tag{1}$$

coupled with the Darcy relation

$$\mathbf{v}(\mathbf{r},t)=-\frac{b^2}{12\mu}\nabla p(\mathbf{r},t). \tag{2}$$

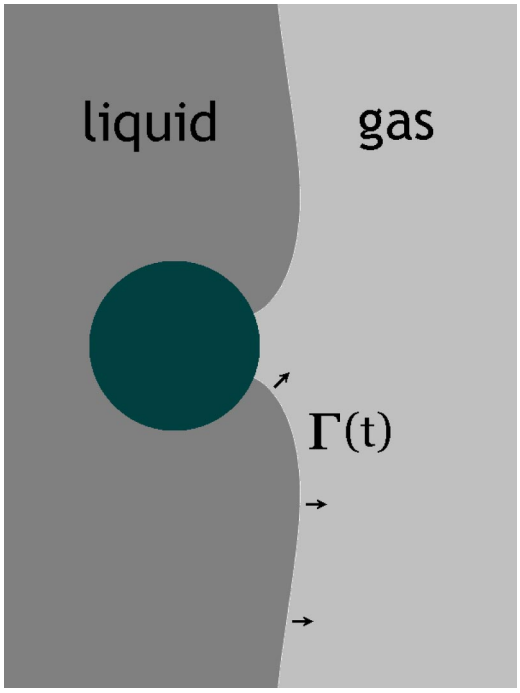

FIG. 1. Moving-boundary-value problem for a liquid-gas interface $\Gamma(t)$ creeping in two dimensions (Hele-Shaw cell) around a solid obstacle.

*Electronic address: vbogoyav@binghamton.edu

In order to specify our dynamic problem, one needs to extend Eqs. (1) and (2) by appropriate boundary conditions applied (i) at the liquid-gas interface, (ii) on the obstacle surface, and (iii) far upstream [6]. We define the kinematics of the liquid-gas interface $\Gamma(t)$ via the normal component ($\mathbf{n}$) of liquid velocity,

$$\frac{\partial \Gamma}{\partial t} \equiv (\mathbf{v})_{\mathbf{n}}, \tag{3}$$

and consider a free surface condition,[1]

$$p|_{\mathbf{r}\in\Gamma(t)} = 0. \tag{4}$$

In the vicinity of the obstacle, we assume a rigidity condition for the velocity field,

$$(\mathbf{v})_{\mathbf{n}} = 0, \tag{5}$$

allowing a free slip of the liquid-gas interface $\Gamma(t)$ on the solid wall.[2] Finally, far upstream we take the most regular case of a uniform flow profile,

$$\mathbf{v}|_{x\to-\infty} = \mathbf{v}_\infty = \text{const}. \tag{6}$$

III. NUMERICAL TECHNIQUE

Solving Eqs. (1)–(6), our ultimate goal consists in tracking the unknown liquid-gas interface Γ, a two-dimensional curve, in time [6]. Although analytical treatments of similar problems by the complex variable techniques have been explored [8,9] and families of rigorous, steady-state solutions have been reported in specific geometries [10–13], for a general free-boundary problem the dynamics $\Gamma(t)$ can hardly be obtained analytically and, therefore, numerical methods of finding a solution must be examined.[3]

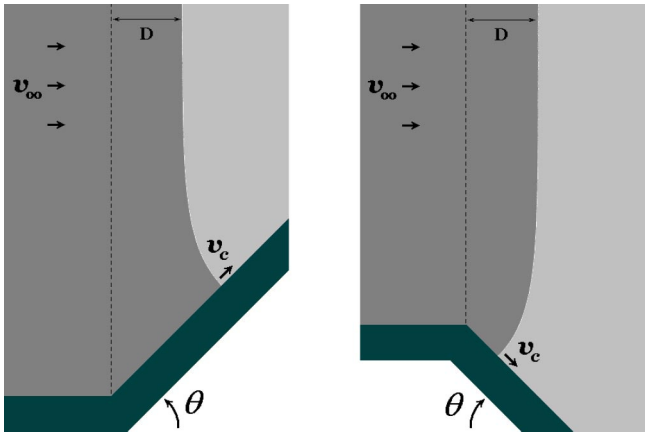

FIG. 2. Free surface Hele-Shaw flows creeping around wedge obstacles of angle θ [narrowing wedge, $\theta>0$ (left); expanding wedge, $\theta<0$ (right)]. Dynamic quantities labeled are a flow velocity at infinity, v_∞; a contact line velocity v_c, and a flow distance at infinity, D.

As an efficient numerical technique, in the present work we apply phase-field *random walk* modeling. Its principal concept, usually referred to as the diffusion-limited aggregation, was introduced by Witten and Sander in 1981 [15], and then proposed for simulations of the free surface flows in Hele-Shaw cells [16]. An original trick in the computation is that Laplace's law for the liquid pressure, $\nabla^2 p = 0$ [Eq. (1)], can be treated stochastically. For that, one would calculate an on-lattice visiting probability P_v for a virtual particle executing a random Brownian walk (i.e., the sequence of discrete diffusion jumps in randomly chosen equivalent lattice directions) within the region of liquid bulk and being adsorbed at the liquid-gas interface $\Gamma(t)$. Upon this particle adsorption, the interface advances by a small step along the external normal; consider the analogy there as $p \leftrightarrow P_v$ [16–22]. Combined with an ensemble averaging to reduce stochastic noise, these random walk schemes have demonstrated their validity and efficiency in modeling two-dimensional free surface flows for both unstable and stable situations [16,23–27]. Here we implement computational algorithms that have been tested to exclude effects of lattice anisotropy and grid size [27].

IV. RESULTS OF SIMULATION

A. Wedge geometry

Let us begin studies of the free surface Hele-Shaw flows with the obstacle geometry of an infinite wedge of angle θ

[1]Equation (4) neglects a contribution from the two-dimensional (x,y) curvature of the interface $\Gamma(t)$. It does not, however, imply that capillary forces naturally existing in the Hele-Shaw cell (between plates) have been excluded. Indeed, these forces are mostly determined by a curvature of the liquid-gas interface in the z dimension, normal to the flow plane. That z curvature represents a constant of the order of $1/b$, so one can subtract the capillary pressure at the moving interface $\Gamma(t)$ from a corresponding value far upstream, $x\to-\infty$, in order to obtain the zero pressure condition as Eq. (4).

[2]This gives us an essentially correct approximation for the cell thickness b much less than the obstacle length scale. For more detailed discussion about actual picture in the obstacle vicinity (wetting region), see Sec. V B.

[3]Clearly nonsteady solutions of the free-boundary problems are to be different from those found for steady-state regimes. A number of investigators have treated steady-state cases for various geometries and initial conditions; while these are of some (mainly mathematical) interest, they do not provide accurate solutions for actual flow problems. The reason is that, in the general case, equipotentials of a steady-state solution do not satisfy the basic kinematic requirement for the moving interface, Eq. (3) [14]. That is to say, if one chooses as an initial condition a shape of the liquid-gas interface Γ that corresponds to an original equipotential of the steady-state solution, the interface will not necessarily follow subsequent equipotentials of that solution.

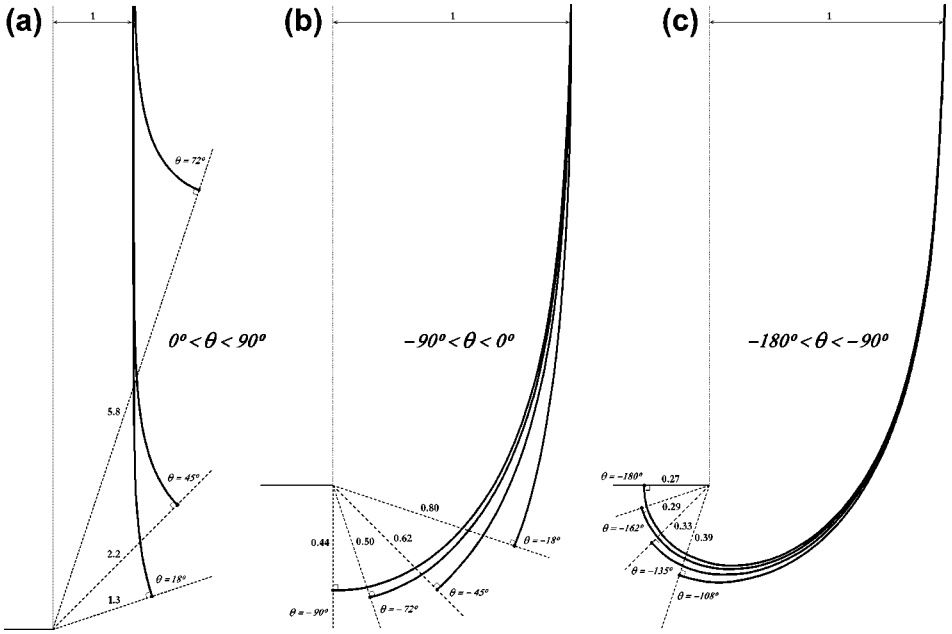

FIG. 3. Quasistationary pictures of a liquid-gas interface Γ (solid curves) creeping around wedge obstacles (dashed lines) of angle θ. (a) Narrowing wedges, $\theta=18°$, 45°, and 72°. (b) and (c) Expanding wedges, $\theta=-18°$, $-45°$, $-72°$, $-90°$, $-108°$, $-135°$, $-162°$, and $-180°$. Ratios of a contact line velocity v_c and a velocity at infinity v_∞ are recorded.

(see Fig. 2). As an initial condition at the wedge origin, we consider the liquid-gas interface Γ to be flat and normal to the flow direction (from left to right). Proceeding to the wedge, the interface becomes globally curved; our goal is to capture this change for various values of the angle $\theta \in (-180°, \ldots, 90°)$.

In Fig. 3, we present results of simulation for a series of wedges; pictures of the liquid-gas interface Γ are shown, as are ratios between velocities at a triple (gas-liquid-solid) contact line (v_c) and at infinity (v_∞ as $y\to\infty$). The ratio v_c/v_∞ gradually increases with the wedge angle θ; for narrowing wedges [$\theta>0$, plot (a)] the contact line moves faster than the interface far away from the obstacle, and for expanding wedges [$\theta<0$, plots (b) and (c)], vice versa. This velocity difference causes complex dynamic shapes (x_i, y_i) of the interface; two specific cases $\theta=-90°$ (“right corner”) and $\theta=-180°$ (“straight edge”) are illustrated in Fig. 4.

A remarkable feature of the wedge geometry is that it yields a quasistationary free-boundary problem. Consider a time-independent flow at infinity, $v_\infty=\text{const}$; this determines

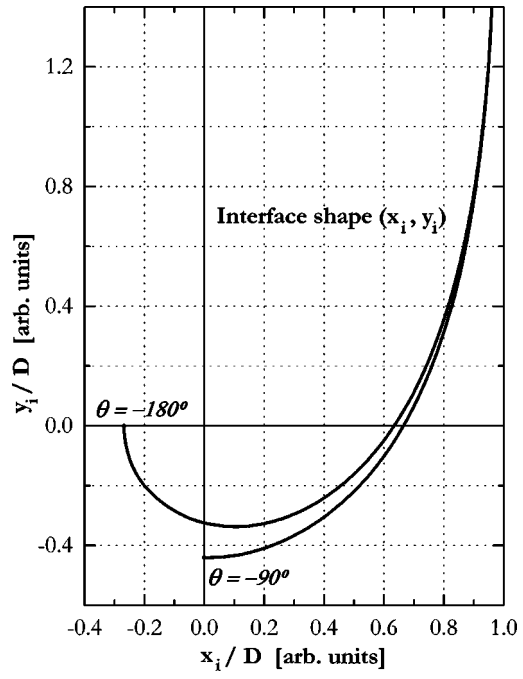

FIG. 4. Quasistationary shape (x_i, y_i) of a liquid-gas interface Γ (normalized to a flow distance at infinity D) for “right corner,” $\theta=-90°$, and “straight edge,” $\theta=-180°$.

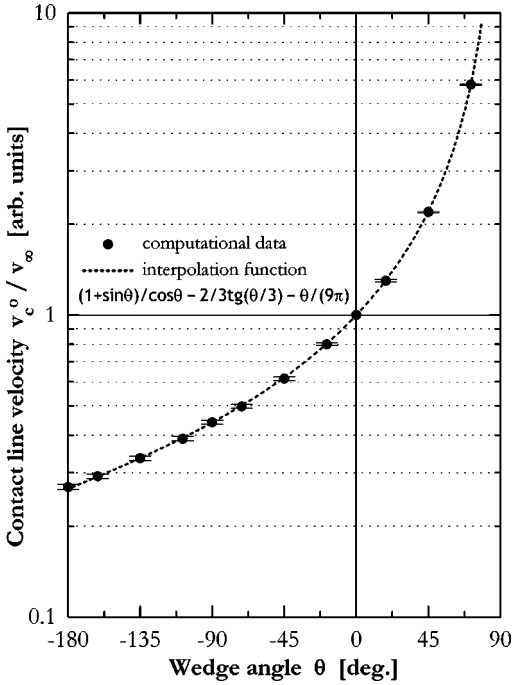

FIG. 5. Scale-invariant contact line velocity v_c^0 (normalized to a flow velocity at infinity, v_∞), as a function of wedge angle $\theta \in (-180°, \ldots, 90°)$. Computational data (solid circles with error bars) are shown together with an interpolation by Eq. (7) (dashed curve).

the interface velocity $\partial\Gamma/\partial t$ as a constant for all corresponding points of Γ. In other words, the wedge flow is a scale invariant and, as a consequence, the contact line velocity $v_c \equiv v_c^0$ divided by v_∞ depends on the wedge angle θ only. This angle dependence has been explored, and results are shown in Fig. 5; our data are well interpolated by the following function (θ values should be substituted in radians):[4]

$$\frac{v_c^0}{v_\infty} = \frac{1+\sin\theta}{\cos\theta} - \frac{2}{3}\tan\left(\frac{\theta}{3}\right) - \frac{\theta}{9\pi}. \tag{7}$$

The connection between v_c^0/v_∞ and θ by Eq. (7) provides us with a basic relation for the free surface Hele-Shaw flows around an obstacle.[5] It will be generalized in subsequent investigations of nonstationary, transient problems below.

B. Step geometry

In order to capture transient regimes of the Hele-Shaw displacement, let us first study free surface flows creeping around a right (down- or up-) step (see Fig. 6). As an initial condition imposed just before a base of the step, we consider the interface Γ to follow the wedge quasistationary behavior [Eq. (7)], i.e., a ''corner'' shape ($\theta=-90°$, Fig. 4) for the down-step and a vertical line ($\theta=0°$) for the up-step. The contact line velocity v_c is expected to undergo singular jumps in both value and course at the base, subject of time and spatial relaxation after that; our goal is to reveal dynamic relations for these down- and up-step transitions.

In Fig. 7, we summarize results of simulation; pictures are shown of the liquid-gas interface Γ evolving in time for the down- [plot (a)] and up-steps [plot (b)]. As seen from plots, this step geometry does raise nonstationary problem; assuming a uniform flow far away from the obstacle, $v_\infty=\text{const}$ as $y\to\infty$, the global interface shape (x_i, y_i) and the contact line velocity v_c are no longer scale invariants but definite functions of the front position (x). Starting from the step base $x=0$, there is a region of singularity as a local interface curvature and the contact velocity v_c go to infinity. This zero neighborhood $(x/h)\to 0$ has been analyzed in detail and, as a result, the following scaling is reported (see Fig. 8):

$$\frac{v_c - v_\infty}{v_\infty} \propto \frac{1}{x^\xi}, \tag{8}$$

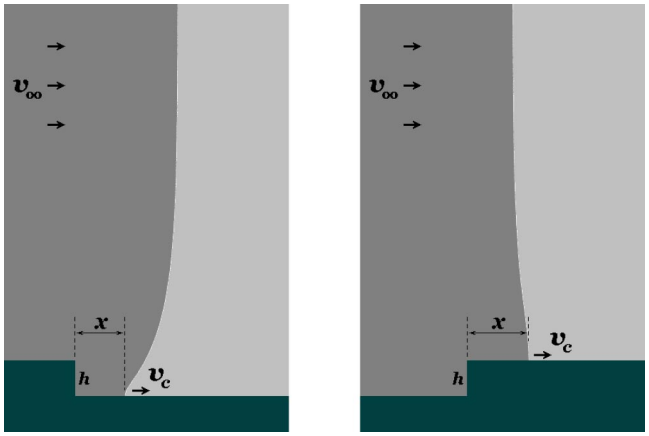

FIG. 6. Free surface Hele-Shaw flows creeping around step obstacles of height h [down-step (left); up-step (right)]. Dynamic quantities labeled are a flow velocity at infinity, v_∞; a contact line velocity v_c; and a front position x.

where $\xi=1$ and 2 for the up- and down-steps, respectively. When the front position x is comparable with the step height (h) and exceeds its value, the liquid-gas interface $\Gamma(t)$ becomes less and less curved (it would apparently relax to a straight line far downstream, $x\to\infty$), whereas the contact velocity v_c converges to v_∞, obeying the relation (see Fig. 9) as

$$\frac{v_c - v_\infty}{v_\infty} \propto \frac{1}{1+\dfrac{x^2}{h^2}}. \tag{9}$$

C. Ellipse geometry

To continue studying transient dynamic regimes of the free surface Hele-Shaw flows, let us consider the obstacle to be an ellipse of anisotropy α (see Fig. 10); this choice extends the preceding step geometry by taking into account smooth, nonsingular solutions. Similar to the wedge configu-

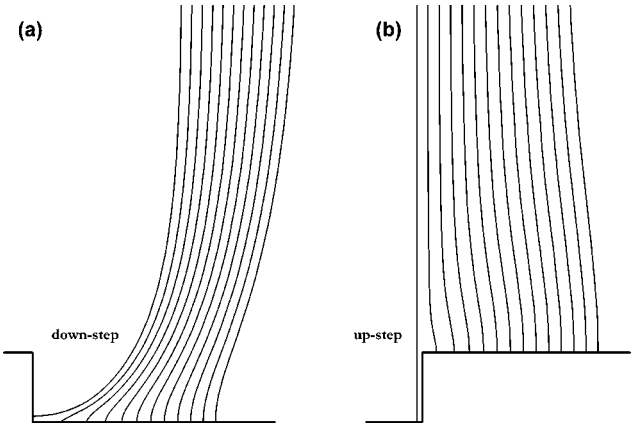

FIG. 7. Dynamic pictures of a liquid-gas interface $\Gamma(t)$ (thin curves) creeping around step obstacles (thick lines): (a) ''down-step'' evolution, (b) ''up-step'' evolution. These pictures are taken in equal time intervals.

[4]In this relation, the first fraction term on the right side is a principal which comes analytically from integral reasons (volume conservation), whereas the other two are empirical corrections required for a better interpolation.

[5]Recently, there has been reported a family of exact solutions for the wedge geometry [13]. These solutions deal with a boundary condition somewhat different from ours: instead of fixing the flow velocity far upstream, at $x\to-\infty$ [Eq. (6)], one fixes a rate of the liquid-gas interface, $\partial\Gamma/\partial t$, at $y\to\infty$. We note that reported solutions give similar results for narrowing wedges ($\theta>0$), but a discrepancy of the order of 10–20 % arises for expanding wedges ($\theta<0$).

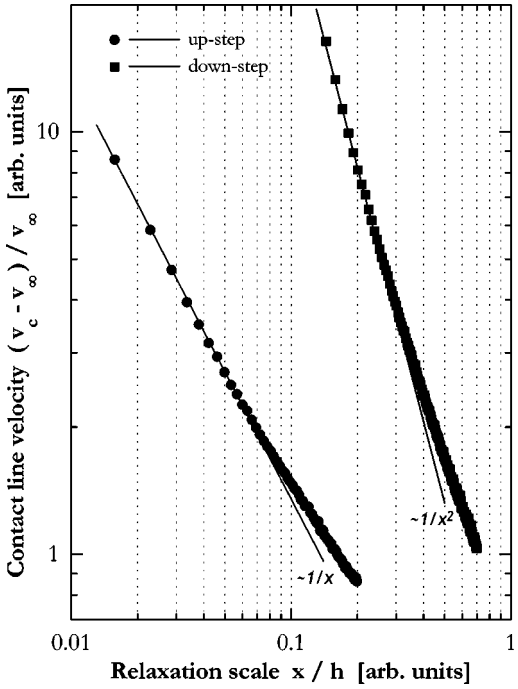

FIG. 8. Increments of contact line velocity v_c (relative and normalized to a flow velocity at infinity, v_∞) as functions of front position x, measured close to step base, $x<h$. Computational data (circles and squares for up- and down-steps, respectively) are approximated by Eq. (8) (solid lines with marks).

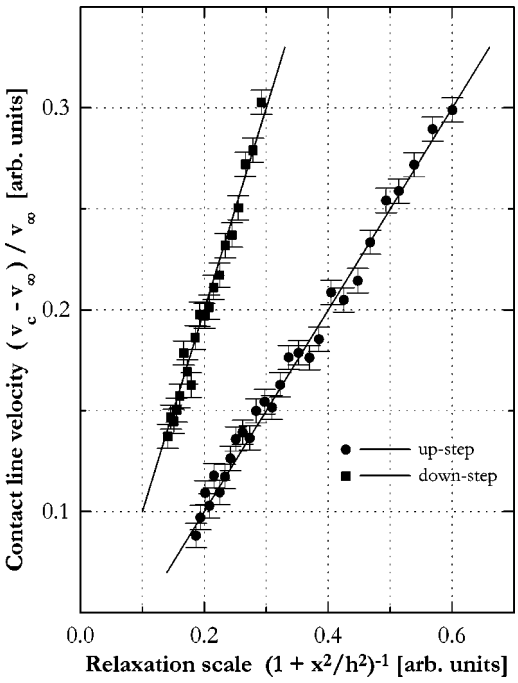

FIG. 9. Increments of contact line velocity v_c (relative and normalized to a flow velocity at infinity, v_∞) as functions of front position x, measured far from step base, $x>h$. Computational data (circles and squares for up- and down-steps, respectively) are approximated by Eq. (9) (solid lines).

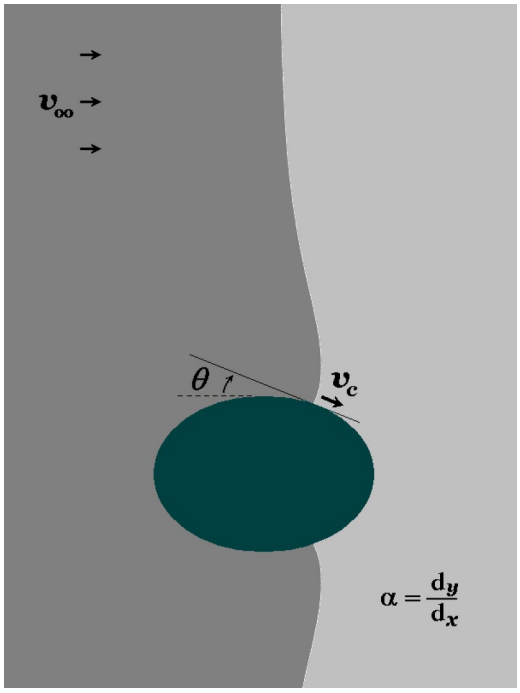

FIG. 10. Free surface Hele-Shaw flow creeping around an ellipse obstacle of anisotropy α (ratio of diameters in y and x directions, d_y/d_x). Dynamic quantities labeled are a flow velocity at infinity, v_∞; a contact line velocity v_c; and a local angle θ.

ration, we fix the liquid-gas interface Γ to be flat and normal to the flow direction in the beginning, just before the obstacle. As the interface creeps around the ellipse, global shape Γ and the contact line velocity v_c become dependent on coordinates of the flow front; our goal is to investigate their functional behavior for various values of the anisotropy coefficient $\alpha \in (0, \ldots, \infty)$.

In Fig. 11, we present results of simulation for two specific cases: $\alpha=1$ ["circle," plot (a)] and $\alpha=\infty$ ["needle," plot (b)]; successive pictures of the liquid-gas interface Γ are shown [due to reflection symmetry of the ellipse geometry, we calculate and draw only half (upper part) of the free surface flow]. As seen from the dynamics, the global interface shape (x_i, y_i) and the contact velocity v_c exhibit rather nonlinear features. The sign of interface curvature is revealed to change twice between the obstacle vicinity and infinity ($y \to \infty$), whereas the contact velocity varies by an order of magnitude at different flow stages. Characterizing these transients, we describe and discuss our data in terms of a local angle θ [measured counterclockwise between the tangent of obstacle surface and the flow direction (from left to right) far from the obstacle, as shown in Fig. 10]; it makes definite analogy to the wedge angle θ (compare with Fig. 2) for nonstationary problems.

In Fig. 12, we plot the θ dependence of the contact velocity v_c with respect to its quasistationary value v_c^0 [Fig. 5, Eq. (7)] for the Hele-Shaw flow around a circle ($\alpha=1$). The increment $(v_c - v_c^0)$ is found to be well interpolated by a cosine function:

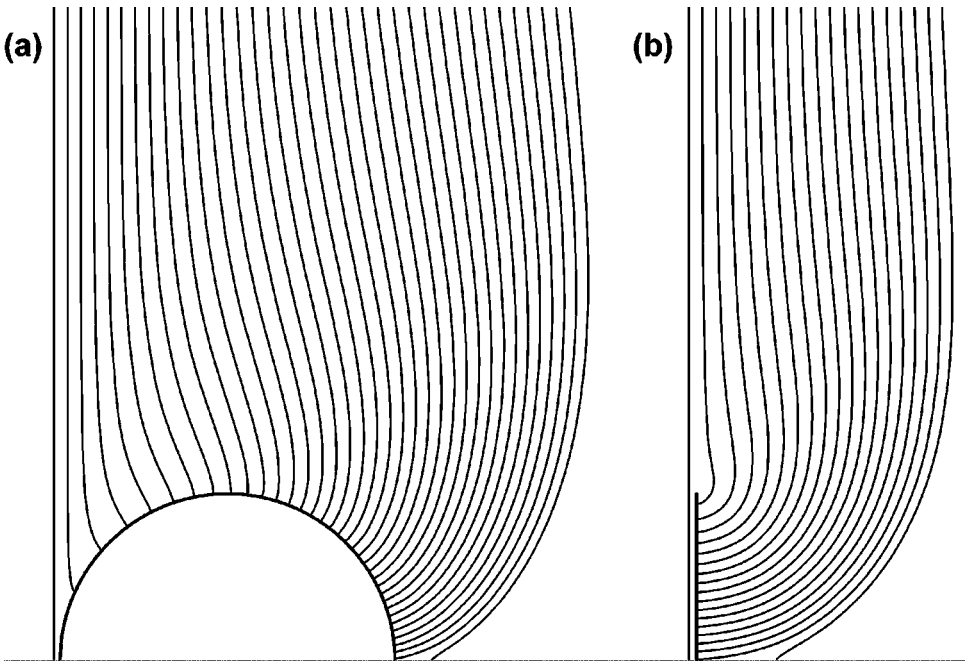

FIG. 11. Dynamic pictures of a liquid-gas interface $\Gamma(t)$ (thin curves) creeping around ellipse obstacles (thick curve/line): (a) ''circle,'' $\alpha=1$ and (b) ''needle,'' $\alpha=\infty$ (horizontal dotted line at the bottom denotes a reflection axis). These pictures are taken in equal time intervals.

$$\frac{v_c - v_c^0}{v_c^0} \propto \cos\theta. \tag{10}$$

As follows from this relation, the difference $(v_c - v_c^0)$ reaches its maximum at the top point of the obstacle ($\theta = 0°$, $v_c^0 = v_\infty$). The dependence on the anisotropy coefficient α has been investigated there, and results are shown in Fig. 13; the relevant velocity increment is reported to be directly proportional to the ellipse anisotropy,

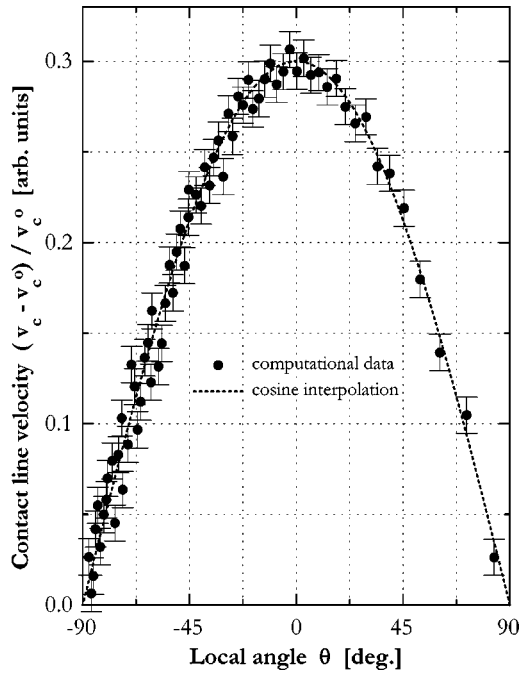

FIG. 12. Increment of contact line velocity v_c (relative and normalized to its quasistationary value v_c^0) as a function of local angle θ, measured for the flow around circle, $\alpha=1$ [Fig. 11(a)]. Computational data (solid circles with error bars) are shown together with an interpolation by Eq. (10) (dashed curve).

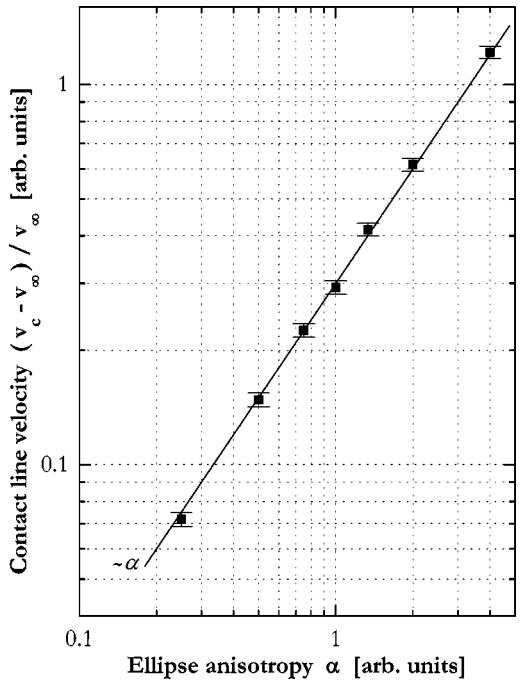

FIG. 13. Increment of contact line velocity v_c (relative and normalized to a flow velocity at infinity, v_∞) as a function of ellipse anisotropy α, measured at top points of obstacles, $\theta=0°$. Computational data for $\alpha=\frac{1}{4}$, $\frac{1}{2}$, $\frac{3}{4}$, 1, $\frac{4}{3}$, 2, and 4 (squares with error bars) are approximated by Eq. (11) (solid line).

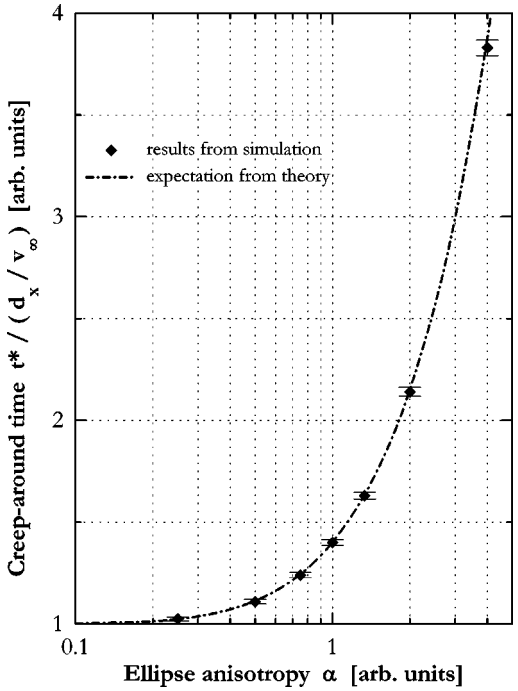

FIG. 14. Time t^* for a liquid-gas interface Γ to creep around an ellipse obstacle (normalized to ratio of diameter d_x and flow velocity at infinity, $v_\infty = \text{const}$) as a function of ellipse anisotropy α. Simulation data for $\alpha = \frac{1}{4}, \frac{1}{2}, \frac{3}{4}, 1, \frac{4}{3}, 2$, and 4 (solid diamonds with error bars) are compared with an expectation from Eq. (14) (dash-dotted curve).

$$\frac{v_c - v_\infty}{v_\infty} = 0.3\alpha. \tag{11}$$

V. DISCUSSION

In the preceding section, we modeled and analyzed the free surface flows that creep in Hele-Shaw cells around solid obstacles of various configurations such as (a) wedges, (b) steps, and (c) ellipses. Now we are going to advance our results; we would, first, derive a more general expression for the contact line velocity v_c and second, consider effects of dynamic wetting in the obstacle vicinity.

A. Contact line velocity formula

Let us introduce the surface of an obstacle in terms of the local angle θ, as we did for the flows around ellipses (Fig. 10). Assuming a Cartesian set of coordinates (x,y), we define the surface curve by an equation $\theta = \theta(x)$ where the angle $\theta \equiv \arctan(\partial y/\partial x)$ and its derivatives $\{\partial\theta/\partial x, \partial^2\theta/\partial x^2, \ldots\}$ are finite and continuous. In further treatments of the contact line velocity v_c with θ as a variable, we primarily consider a zero- ($\theta = \text{const}$) and a first-order (finite $\theta' \equiv \partial\theta/\partial x$) contribution,

$$v_c = v_c^0[1 + \mathcal{K}(\theta, \theta')]. \tag{12}$$

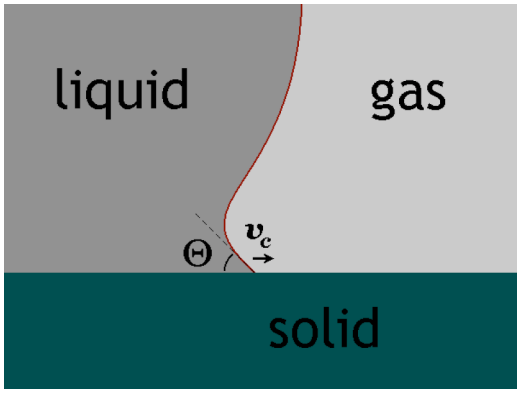

FIG. 15. Wetting phenomena in vicinity of a triple (gas-liquid-solid) contact line. Dynamic quantities labeled are a contact line velocity v_c and a wetting angle Θ.

Here the quasistationary factor v_c^0 (for $\theta = \text{const}$) is governed by Eq. (7), and $\mathcal{K}$ represents a θ' correction obeying the relation[6]

$$\mathcal{K}(\theta, \theta') = \Omega(\theta)(|y\theta'|^\gamma), \tag{13}$$

where we suggest and separate the angle $[\Omega(\theta)]$ and the derivative $[|y\theta'|^\gamma]$ dependencies.

The unknown function $\Omega(\theta)$ and the exponent value γ in Eq. (13) can be determined from our data obtained for the ellipse obstacles (Sec. IV C) as follows. Considering first the Hele-Shaw flow around a circle [$\alpha = 1$; Fig. 11(a)], $y = (1 - x^2)^{1/2}$, we set $|y\theta'| \equiv 1$, i.e., the cosine relation by Eq. (10) (see Fig. 12) is substituted for $\Omega(\theta)$. Next, for a regular ellipse $y = \alpha(1 - x^2)^{1/2}$, at the top point of its surface ($x = 0$, $\theta = 0°$) we have $\Omega \equiv 1$ and $|y\theta'|^\gamma = \alpha^{2\gamma}$. Since the corresponding increment of the contact velocity v_c is proportional to α [Eq. (11); Fig. 13], we need to fix the exponent γ at 1/2, so we finally derive the contact line velocity as

$$v_c = v_c^0[1 + 0.3\cos\theta\sqrt{|y\theta'|}]. \tag{14}$$

Coupled with Eq. (7) in Sec. IV A, this formula essentially connects the local (v_c) and the global (v_∞) properties of the free surface Hele-Shaw flows we have considered.

In order to provide a test for the validity of the expression above, we have calculated the times t^* for free surface flows to creep around ellipse obstacles of various anisotropies by a numerical integration of Eq. (14) along the obstacle surface, and then compared these calculations with actual data from the random walk simulations; corresponding results are shown in Fig. 14. As seen, the theoretical expectation precisely describes the simulations in a rather wide range of the anisotropy coefficient, $\alpha \in (1/4, \ldots, 4)$, i.e., for most of the

[6]This specific form for the θ' correction is suggested by the analysis of data for flows around steps—see the relaxation scale by Eq. (9) in Sec. IV B—the increments of the contact velocity v_c depend on the term $1/(1 + x^2/h^2) = h[\arctan(x/h)]'$ which has an equivalent for the continuous case ($h \leftrightarrow y$) as $y\theta'$. The absolute notation $|y\theta''|$ is used in Eq. (13) since the velocity increments are always positive (Fig. 9).

ellipse family. This allows us to conclude that Eq. (14) appears to be appropriate at least for *any convex geometry* of the obstacle surface.

B. Consideration of dynamic wetting

In modeling the Hele-Shaw flows around obstacles, we originally imposed free slip of the liquid-gas interface $\Gamma(t)$ at solid boundaries [rigidity condition by Eq. (5)]. This is, however, true only if we exclude from quantitative description a wetting region (with a lengh scale of the order of cell thickness b) in the obstacle vicinity (see Fig. 15). Inside that region the interface shape is known to deviate from the free-slip solutions, making a wetting angle Θ which depends on dynamics of the contact line, $v_c(t)$ [28,29].

The governing function for the wetting angle Θ is generally given by a capillary number Ca defined as

$$\mathrm{Ca} \equiv \frac{\mu v_c}{\sigma}, \tag{15}$$

where σ is the coefficient of liquid-gas interphase tension. Considering knowledge of the parameter Ca for a free surface Hele-Shaw flow from Eqs. (7), (14), and (15), dynamic wetting angle Θ in the three-phase system is described by an experimental Hoffman's relation [30]:

$$\frac{\cos\Theta_e - \cos\Theta}{\cos\Theta_e + 1} = \tanh[4.96(\mathrm{Ca})^{0.702}]. \tag{16}$$

Here Θ_e denotes a static angle (corresponding to the thermodynamic equilibrium, $v_c = 0$) by the Young law [29]

$$\cos\Theta_e = \frac{\sigma_{SG} - \sigma_{SL}}{\sigma} \tag{17}$$

(σ_{SG} and σ_{SL} are solid-gas and solid-liquid interphase tensions, respectively).

Thus one would explicitly determine the wetting angle Θ at each time moment for the free surface Hele-Shaw flows around an obstacle from Eqs. (15)–(17). After that, in vicinity of the obstacle one can estimate and apply local corrections to the free-slip solutions $\Gamma(t)$ [28].

VI. CONCLUSION

By a random walk computational technique, we have investigated the free surface Hele-Shaw flows driven around solid obstacles by a uniform pressure gradient far upstream. We have characterized the time and spatial evolution (on both short and long scales) of a liquid-gas interface creeping around obstacles as wedges, steps, and ellipses. Particular attention has been addressed to the dynamics of a triple (gas-liquid-solid) contact line for which we have derived a functional relationship with the local geometry of obstacles. Besides, wetting phenomena in the obstacle vicinity have been considered.

ACKNOWLEDGMENTS

We would like to thank Professor J. Geer for fruitful discussions on the subject. This research was supported in part by the National Science Foundation, Grant No. DMII-9908332. One of us (V.A.B.) also acknowledges the funding provided by a grant from Corning, Inc.

[1] H.J.S. Hele-Shaw, Nature (London) **58**, 34 (1898).
[2] For a review, see D. Bensimon, L.P. Kadanoff, S. Liang, B.I. Shraiman, and C. Tang, Rev. Mod. Phys. **58**, 977 (1986); A. Oron, S.H. Davis, and S.G. Bankoff, *ibid.* **69**, 931 (1997); *Dynamics of Curved Fronts*, edited by P. Pelcé (Academic, Orlando, 1988), and references therein.
[3] Lord Rayleigh, Proc. London Math. Soc. **XIV**, 170 (1883).
[4] G.I. Taylor, Proc. R. Soc. London, Ser. A **201**, 192 (1950).
[5] P.G. Saffman and G.I. Taylor, Proc. R. Soc. London, Ser. A **245**, 312 (1958).
[6] J. Crank, *Free and Moving Boundary Problems* (Oxford University Press, Oxford, 1984).
[7] See, e. g., G.L. Lehmann, T. Driscoll, N.R. Guydosh, P.C. Li, and E.J. Cotts, IEEE Trans. Compon., Packag. Manuf. Technol., Part A **21**, 266 (1998).
[8] S. Richardson, J. Fluid Mech. **56**, 609 (1972); **102**, 263 (1981).
[9] S.D. Howison, Eur. J. Appl. Math. **3**, 209 (1992); L.J. Cummings, S.D. Howison, and J.R. King, *ibid.* **10**, 635 (1999).
[10] S.D. Howison and J.R. King, IMA J. Appl. Math. **42**, 155 (1989).
[11] C. Huntingford, Comput. Math. Appl. **29**, 45 (1995).
[12] L.J. Cummings, Eur. J. Appl. Math. **10**, 547 (1999).
[13] S. Richardson, Eur. J. Appl. Math. **12**, 665 (2001); **12**, 677 (2001).
[14] J. Geer (private communication).
[15] T.A. Witten and L.M. Sander, Phys. Rev. Lett. **47**, 1400 (1981); Phys. Rev. B **27**, 5686 (1983).
[16] C. Tang, Phys. Rev. A **31**, 1977 (1985).
[17] L. Paterson, Phys. Rev. Lett. **52**, 1621 (1984).
[18] L.P. Kadanoff, J. Stat. Phys. **39**, 267 (1985).
[19] Z. Koza, J. Phys. A **24**, 4895 (1991).
[20] M. Sahimi, Rev. Mod. Phys. **65**, 1393 (1993).
[21] B.K. Johnson and R.F. Sekerka, Phys. Rev. E **52**, 6404 (1995).
[22] T.C. Halsey, Phys. Today **53(11)**, 36 (2000).
[23] S. Liang, Phys. Rev. A **33**, 2663 (1986).
[24] P. Meakin, F. Family, and T. Vicsek, J. Colloid Interface Sci. **117**, 394 (1987); T. Vicsek, Phys. Scr., T **19**, 334 (1987).
[25] J.F. Fernández and J.M. Albarrán, Phys. Rev. Lett. **64**, 2133 (1990); H. La Roche, J.F. Fernández, M. Octavio, A.G. Loeser, and C.J. Lobb, Phys. Rev. A **44**, R6185 (1991).
[26] A. Arnéodo, Y. Couder, G. Grasseau, V. Hakim, and M. Rabaud, Phys. Rev. Lett. **63**, 984 (1989); A. Arnéodo, J. Elezgaray, M. Tabard, and F. Tallet, Phys. Rev. E **53**, 6200 (1996).
[27] V.A. Bogoyavlenskiy, Phys. Rev. E **63**, 045305(R) (2001); **64**, 066303 (2001).
[28] E.B. Dussan V and S.H. Davis, J. Fluid Mech. **65**, 71 (1974); E.B. Dussan V, Annu. Rev. Fluid Mech. **11**, 371 (1979).
[29] P.G. de Gennes, Rev. Mod. Phys. **57**, 827 (1985).
[30] R. Hoffman, J. Colloid Interface Sci. **50**, 228 (1975).